Available online at www.sciencedirect.com
ScienceDirect
International Journal of Pharmaceutics 328 (2007) 112–118
INTERNATIONAL JOURNAL OF PHARMACEUTICS
www.elsevier.com/locate/ijpharm

Conformational polymorphism in bicalutamide

Daniel R. Vega [a,b,*], Griselda Polla [a], Andrea Martinez [c], Elsa Mendioroz [a], María Reinoso [a]

[a] *Unidad de Actividad Física, Comisión Nacional de Energía Atómica, Av. Gral. Paz 1499, 1650 San Martín, Buenos Aires, Argentina*
[b] *Escuela de Ciencia y Tecnología, Universidad Nacional de General San Martín, Calle 91 3391, 1653 San Martín, Buenos Aires, Argentina*
[c] *Cátedra de Química Orgánica III, Departamento de Química Orgánica, Facultad de Farmacia y Bioquímica, Universidad de Buenos Aires, Argentina*

Received 29 March 2006; received in revised form 1 August 2006; accepted 2 August 2006
Available online 8 August 2006

Abstract

Two crystalline forms (forms I and II) and an amorphous phase of bicalutamide were fully characterized through combined results of differential scanning calorimetry, X-ray powder and single crystal diffraction and Raman spectroscopy. Each polymorph crystallizes with one molecule in the asymmetric unit and the molecular conformations are quite different between them. The main difference is provided by C12–C11–S8–C5 torsion angle, which assumes a value of −88.3(4)° (−Syn–Clinal) and 72.5(4)° (+Syn–Clinal) in forms I and II, respectively. Consequently, molecules in form I show an open folding and molecules in form II a closed one. The relative stability between forms I and II is presented in an energy versus temperature diagram, where forms I and II are considered as a monotropic system, being form I the more stable one. The amorphous phase was observed very metastable and it converts to form II spontaneously at RT in around a week

Keywords: Bicalutamide; Polymorphism; Stability; Crystal structure; Thermal analysis

1. Introduction

Organic compounds can crystallize in more than one crystal form. The ability of a substance to exist in several different forms is known as polymorphism. If crystals of pharmaceuticals exhibit polymorphism, their physical properties such as density, melting point, solubility and then stability, bioavailability and processibility could be different between different polymorphs. From some particular point of view, pharmaceutical polymorphism can be considered as part of the crystal engineering area (Haleblian and McCrone, 1969) and it allows a safe manipulation of the crystal properties of solids (Caira, 1998). The importance of polymorphism knowledge for pharmaceutical industry lies on having reliable and robust processes; accordingly with GMP, polymorphism studies are considered a regulatory requirement. For pharmaceutical polymorphism the structure–property relationships are mainly governed by differences in the spatial arrangement of the constituent molecules in the crystal, and in some cases, by variations in molecular conformation.

Bicalutamide (Scheme 1) is a pharmaceutically active compound that possesses antiandrogenic activity. Such a compound is very useful in treating prostate cancer. Several patents describe methods to produce crystalline material and evidence of polymorphism (US Patent, 2004; WO A1 Patent, 2004; WO A2 Patent, 2004). Accordingly to our results, bicalutamide is practically insoluble in water (less than 40 mg/l), so it could belong to class II of the biopharmaceutics classification systems (BCS) and then studies on polymorphism became essential for this compound. Bicalutamide presents an additional interesting point of view because it is a flexible molecule and the crystallization of conformationally flexible molecules has two potential complications not encountered by rigid molecules, namely, conformational polymorphism and reduced crystallization tendency (Yu et al., 2000).

In the present work we have focused our interest on the stability of the two bicalutamide crystalline forms and an amorphous phase, providing some physical information that supports our final energy versus temperature stability diagram interpretation.

During the thermal studies, a metastable amorphous phase could be produced (WO A1 Patent, 2004), which was very important to obtain seeds of form II.

The behaviours of form I and II were fully characterized through differential scanning calorimetry (DSC). The combined

* Corresponding author at: Unidad de Actividad Física, Comisión Nacional de Energía Atómica, Av. Gral. Paz 1499, 1650 San Martín, Buenos Aires, Argentina. Tel.: +54 11 6772 7107; fax: +54 11 6772 7121.
E-mail address: vega@cnea.gov.ar (D.R. Vega).

0378-5173/$ – see front matter © 2006 Elsevier B.V. All rights reserved.
doi:10.1016/j.ijpharm.2006.08.001

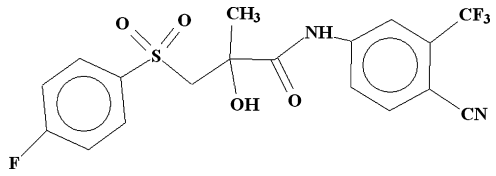

Scheme 1. Drawing of bicalutamide molecule.

results of X-ray powder (XRPD) and single crystal diffraction and Raman spectroscopy (RS) as applied to the forms I and II are reported herein.

2. Experimental

2.1. Materials

Crystalline material of bicalutamide (empirical formula: C18 H14 F4 N2 O4 S, formula weight: 430.37) was obtained as form I by recrystallization from ethanol solution (99.9%) by dissolving 5 mg of bicalutamide in 10 ml of solvent at room temperature (25(2) °C) and at 40(2) °C. Form I was obtained as plates at room temperature and needles at 40 °C. Amorphous material was produced cooling down to RT melted material of form I. Form II was generated by transforming amorphous material. Powder of form II was obtained by seeding form II in a saturated ethanol solution at 40(2) °C.

2.2. Methods

Raman spectroscopy was performed using a Jarrell-Ash 25–300 spectrometer with an Ar^+ laser operating at 514.5 nm; the dispersed beam was analyzed in an 90° geometry.

X-ray powder diffraction (XRPD) patterns were recorded on a X'Pert Philips PW3020 diffractometer (Philips, The Netherlands) over the 2θ range of 5–40°, using graphite monochromatized Cu Kα radiation (1.54184 Å), in aluminium sample holders, at room temperature (1° divergence slit; 1° detector slit and 0.1 mm receiving slit, scanning step 0.02°, counting time 2 s). Suitable samples for XRPD measurement were obtained by grinding crystalline material in an agate mortar, particle size around 5 μm.

Single crystal X-ray diffraction data were collected at room temperature (25(2) °C), using monochromatized Mo Kα radiation (0.71073 Å), on an AFC6S (Rigaku Corporation, Japan) diffractometer for forms I and II. Data-collection strategy and data reduction followed standard procedures implemented in the MSC/AFC (1993).

The structures were solved using program SHELXS-97 (Sheldrick, 1997) and refined using the full-matrix LS procedure with SHELXL-97 (Sheldrick, 1997). Anisotropic displacement parameters were employed for non-hydrogen atoms and H atoms were treated isotropically with $U_{iso} = 1.2$ (for those attached to aromatic carbons and to the N atom) or 1.5 times (for those bonded to methyl carbons) the U_{eq} of the parent atoms. All H atoms were located at the expected positions and they were refined using a riding model. Routines employed to create CIF files are from WinGX package (Farrugia, 1999).

Crystallographic data (excluding structure factors) for both forms have been deposited with the Cambridge Crystallographic Data Centre as supplementary publication nos. CCDC 602632 and 602633.

Differential scanning calorimetry (DSC) was carried out with a Shimadzu DSC-60 instrument (Shimadzu, Kyoto, Japan). Samples weighting 3–5 mg were heated in opened aluminum pans at a rate of 10 K/min under nitrogen gas flow of 35 ml/min.

Polarized thermomicroscopy was performed using a Kofler hot stage (Thermovar, Reichert, Vienna, Austria) in a Ortholux II POL-BK microscope (Leitz-Wetzlar, Germany) and an on-purpose adapted webcam.

UV–vis absorbance was measured using a Shimadzu UV-160A spectrophotometer (Shimadzu, Kyoto, Japan) in the range 200–400 nm using a quartz recipient with an optical pathway of 1 cm. *Saturated water solutions*: Saturated solutions of forms I and II were generated by placing an excess amount of sample (52 mg) in 500 ml of water. The suspension was stirred during 2 h at room temperature (25(2) °C) and the final suspensions were filtered using 0.45 μm Millipore filter (final measured pH 5). No extra dilution was necessary.

3. Results

3.1. Structure analysis

As stated, single crystals of forms I and II were obtained and both crystal structures were solved. Table 1 presents some relevant crystallographic and refinement data, Table 2 introduces selected structural parameters, and Table 3, the geometric description for hydrogen bond interactions following the criteria: H···A distance < r(A) + 2 Å and D–H···A angle > 110° (A: acceptor and D: donor).

Each polymorph crystallizes with one molecule in the asymmetric unit ($Z' = 1$), as shown in Figs. 1 and 2. These molecules exhibit quite different conformation. The main difference is provided by C12–C11–S8–C5 torsion angle, which assumes a value of −88.3(4)° (−Syn–Clinal) and 72.5(4)° (+Syn–Clinal)

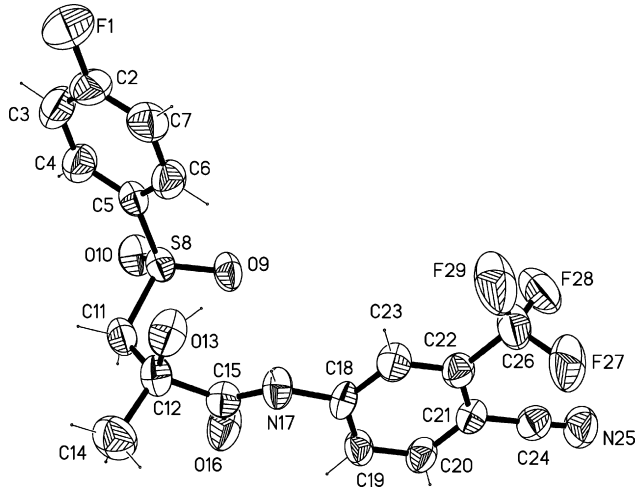

Fig. 1. Bicalutamide form I showing the numbering scheme used and displacement ellipsoids drawn at the 50% probability level.

Table 1
Crystal data and structure refinement for bicalutamide

	Form I	Form II
Crystal system	Monoclinic	Triclinic
Space group	$P2_1/c$	P-1
Unit cell dimensions	$a = 14.997(3)$ Å, $\alpha = 90°$; $b = 12.244(2)$ Å, $\beta = 104.67(3)°$; $c = 10.483(2)$ Å, $\beta = 90°$	$a = 7.822(1)$ Å, $\alpha = 88.19(3)°$; $b = 11.060(2)$ Å, $\beta = 77.03(3)°$; $c = 11.324(2)$ Å, $\gamma = 77.96(3)°$
Volume	1862.2(6) Å^3	933.6(3) Å^3
Z	4	2
Density (calculated)	1.535 g/cm^3	1.531 g/cm^3
Absorption coefficient	0.241 mm^{-1}	0.241 mm^{-1}
$F(0\,0\,0)$	880	440
Crystal size	0.2 mm × 0.2 mm × 0.3 mm	0.2 mm × 0.3 mm × 0.4 mm
Theta range for data collection	2.18–25.99°	1.85–26.00°
Index ranges	$-18 \le h \le 18$, $-15 \le k \le 1$, $-1 \le l \le 12$	$-9 \le h \le 7$, $-13 \le k \le 1$, $-13 \le l \le 13$
Reflections collected	4679	3802
Independent reflections	3651 [R(int) = 0.0960]	3347 [R(int) = 0.0310]
Completeness to $\theta = 25.99°$	100.0%	91.3%
Refinement method	Full-matrix least-squares on F^2	Full-matrix least-squares on F^2
Data/restraints/parameters	3651/0/264	3347/0/264
Goodness-of-fit on F^2	0.969	1.043
Final R indices [$I > 2\sigma(I)$]	$R1 = 0.0675$, w$R2 = 0.1575$	$R1 = 0.0629$, w$R2 = 0.1694$
R indices (all data)	$R1 = 0.2129$, w$R2 = 0.2045$	$R1 = 0.1478$, w$R2 = 0.2030$
Largest diff. peak and hole	0.267 and −0.382 e Å^{-3}	0.405 and −0.379 e Å^{-3}

in forms I and II, respectively. Consequently, molecules in form I show an open folding (Fig. 1) and molecules in form II a closed one (Fig. 2). The conformational differences are better observed in Fig. 3, where the six membered ring C2/C3/C4/C5/C6/C7 of molecules of form I and II were overlapped using least squares fit (XP in SHELXTL/PC) (Sheldrick, 1994). The molecular conformation is also stabilized by very weak intramolecular hydrogen bonds (Table 3). In both molecules (form I and II), N17 is a hydrogen bond donor to O13. However, C19–H19···O16 is observed in form I and C23–H23···O16 in form II. The fact that O16 is involved in different hydrogen interaction may be due to the difference observed in the C19–C18–N17–C15 torsion angle value (−28.5(4)° (−Syn–Periplanar) and −164.4(4)° (−Anti–Periplanar) in forms I and II, respectively).

The crystal cohesion is mainly provided by intermolecular hydrogen bond interactions (Table 3). Molecules in form I are arranged as chains generated by a bifurcated hydrogen bond involving H13 (Fig. 4) in which O16 and O19 act as receptors in the neighbouring symmetry-related molecule. Molecules in form II pack as chains of dimers: two molecules are linked to each other through two very weak hydrogen bonds where N17 acts as a donor and O10 as an acceptor, determining a dimer. Then, each dimer interacts with its [−1 + x, 1 + y, z] translated by a hydrogen bond involving H13 (Fig. 5)

Table 2
Selected bond lengths (Å), angles (°) and torsion angles (°) for bicalutamide

	Form I	Form II
C(5)–S(8)	1.761(5)	1.753(4)
C(11)–C(12)	1.494(7)	1.498(6)
C(11)–S(8)	1.793(5)	1.800(5)
C(12)–O(13)	1.442(6)	1.454(5)
C(12)–C(14)	1.513(8)	1.509(7)
C(12)–C(15)	1.548(8)	1.545(6)
C(15)–O(16)	1.212(6)	1.216(5)
C(15)–N(17)	1.350(6)	1.351(5)
C(18)–N(17)	1.413(6)	1.406(5)
O(9)–S(8)	1.433(4)	1.427(4)
O(10)–S(8)	1.446(4)	1.423(5)
C(12)–C(11)–S(8)	116.4(4)	121.0(4)
O(13)–C(12)–C(14)	110.2(4)	108.4(4)
C(11)–C(12)–C(15)	110.4(4)	111.8(4)
O(16)–C(15)–N(17)	125.1(5)	124.6(4)
N(17)–C(15)–C(12)	114.9(5)	115.2(4)
C(15)–N(17)–C(18)	126.8(4)	127.8(3)
O(9)–S(8)–O(10)	118.3(2)	119.6(3)
C(5)–S(8)–C(11)	108.3(2)	106.1(2)
S(8)–C(11)–C(12)–C(15)	−64.2(5)	−65.6(5)
C(11)–C(12)–C(15)–N(17)	130.2(5)	128.8(4)
C(12)–C(15)–N(17)–C(18)	−175.1(5)	178.2(4)
C(12)–C(11)–S(8)–C(5)	−88.3(4)	72.5(4)
C(19)–C(18)–N(17)–C(15)	−28.5(4)	−164.4(4)

Table 3
Geometric description for hydrogen bond interactions

Donor–H···acceptor	D–H (Å)	H···A (Å)	D···A (Å)	D–H···A (°)
Form I				
O(13)–H(13)···O(9)[a]	0.820	2.475	2.864(7)	110.24
O(13)–H(13)···O(16)[a]	0.820	2.568	3.370(7)	166.36
N(17)–H(17)···O(13)	0.860	2.148	2.595(6)	111.94
C(19)–H(19)···O(16)	0.930	2.387	2.899(6)	114.49
Form II				
O(13)–H(13)···N(25)[b]	0.820	2.173	2.986(6)	171.43
N(17)–H(17)···O(10)[c]	0.860	2.384	3.147(6)	148.07
N(17)–H(17)···O(13)	0.860	2.099	2.577(5)	114.51
C(23)–H(23)···O(16)	0.930	2.236	2.837(5)	121.67

[a] Symmetry code for acceptor atom is: (x, 3/2 − y, 1/2 + z).
[b] Symmetry code for acceptor atom is: (−1 + x, 1 + y, z).
[c] Symmetry code for acceptor atom is: (1 − x, 2 − y, −z).

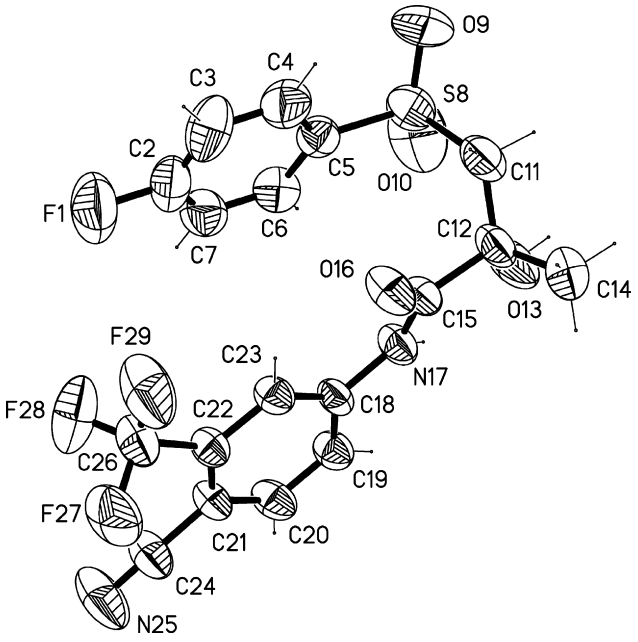

Fig. 2. Bicalutamide form II showing the numbering scheme used and displacement ellipsoids drawn at the 50% probability level.

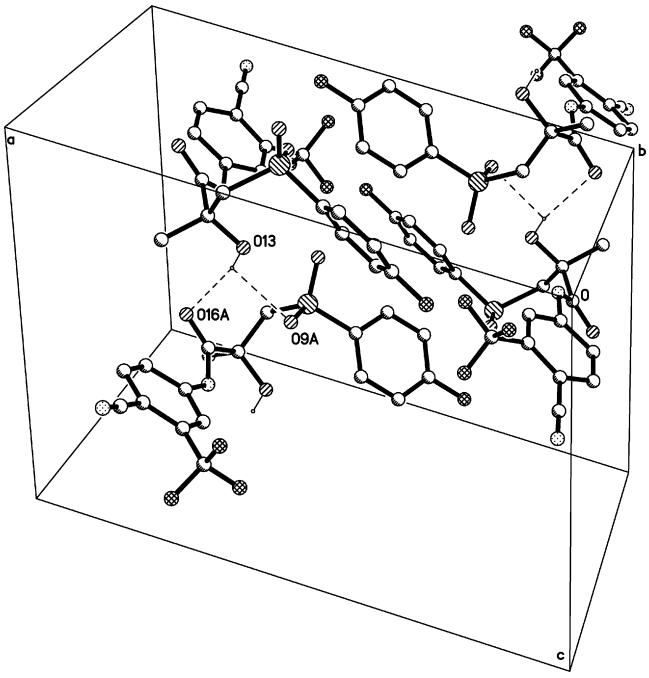

Fig. 4. Packing diagram of bicalutamide form I showing the intermolecular hydrogen bonds represented as dashed lines. (Only H atoms involved in these intermolecular interactions are drawn.)

in which N25 is the acceptor, determining a chain. Moreover, the closed folding of molecules of form II allows them to have an extra rather weak $\pi\cdots\pi$ interaction between the six membered ring C2/C3/C4/C5/C6/C7 and the six membered ring C18/C19/C20/C21/C22/C23 belonging to the next molecule translated along the crystallographic a axis, with a center–center distance of 3.890(3) Å and a slippage angle of 18.25° between cycles, providing further cohesion to the crystal packing.

From the structural models, X-ray powder diffraction diagrams were calculated and compared with the experimental ones, showing good agreement between them (Fig. 6).

The structural studies were complemented by vibrational characterization through Raman spectroscopy. Fig. 7 shows the Raman spectra for forms I and II, where a characteristic maximum is observed for form I at very low wavenumber (around 150 cm^{-1}) and three characteristic maxima appear for form II (around 600, 1450 and 1700 cm^{-1}). The first observed difference were found below 400 cm^{-1}, a region very useful to distinguish between polymorphs due to the fact that differences on backbone deformations, librations and lattice vibrations appear in this region. Moreover, as expected in this case because of the conformational polymorphism, some other differences were observed in a medium region (between 500 and 1700 cm^{-1}) as a fingerprint that provides several features to distinguish between both polymorphs.

3.2. Thermal studies

DSC studies of both crystalline forms presented similar thermal behaviours as shown in Fig. 8. Both diagrams show endothermic peaks, none of which is related to weight loss as

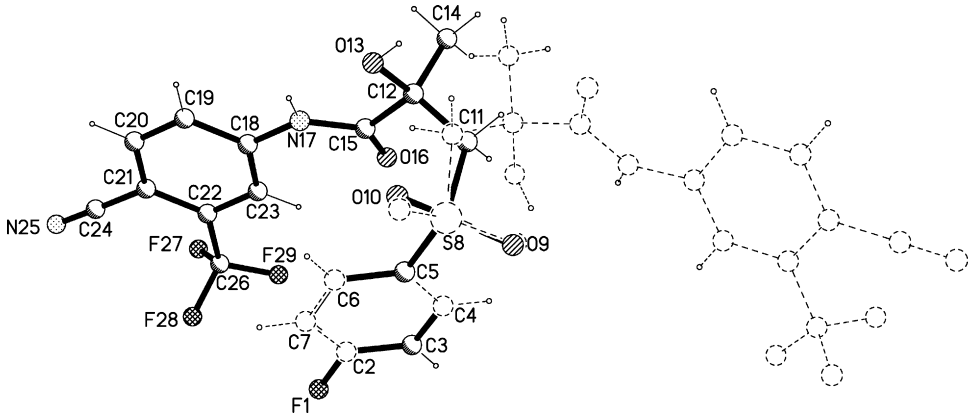

Fig. 3. Least squares overlap of the six membered ring C2/C3/C4/C5/C6/C7 of molecules of form I (dashed lines, open folding) and form II (bold lines, closed folding) to show the differences between them.

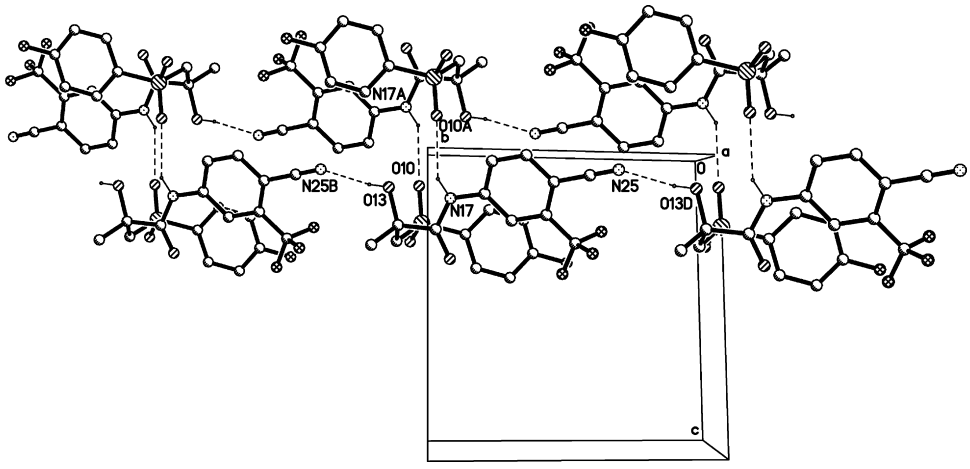

Fig. 5. Packing diagram of bicalutamide form II showing the intermolecular hydrogen bonds represented as dashed lines. (Only H atoms involved in these intermolecular interactions are drawn.)

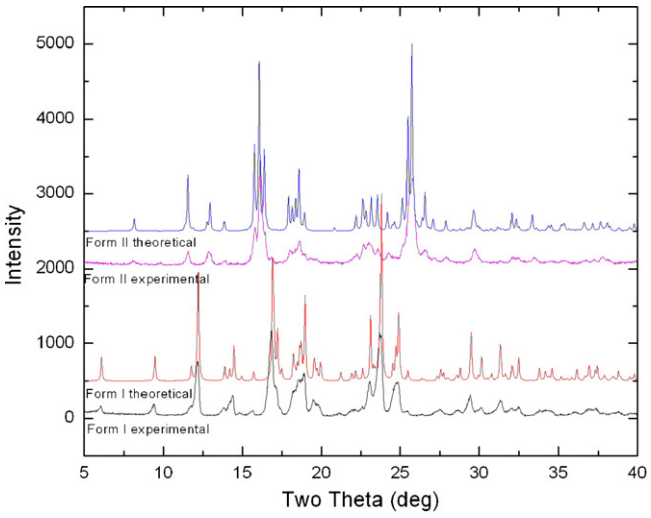

Fig. 6. Calculated and experimental XRPD patterns of form I (bottom) and form II (top).

checked by TG analysis. In both forms, the transitions with T_{onset} about 192 and 189 °C are related to melting points of forms I ($T_{fusion\,I}$) and II ($T_{fusion\,II}$), respectively, with latent heat of about 111 J/g ($\Delta H_{(I)\text{-}Liq}$) for the former and 100 J/g ($\Delta H_{(II)\text{-}Liq}$) for the latter.

After melting form I, the sample can be quenched cooling down to room temperature and so an amorphous phase is produced. This behaviour was also confirmed by visual observation under thermal stage polarizing microscope. When heating the amorphous phase, a glass transition occurs around 50 °C (see Fig. 8). Heating on, the amorphous phase suffers a transformation (solid or cold crystallization) to form II through an exothermal solid–solid transition around 105 °C ($T_{amorphous\,II}$) which involves a latent heat of about 71 J/g ($\Delta H_{amorphous\,II}$). After this event, the sample finally melts at the form II melting point ($T_{fusion\,II}$). The solid–solid transition described above was also checked by XRPD quenching a sample after this exothermic transformation occurred. This method is the obvious way to obtain bicalutamide form II for seeding purposes as we do.

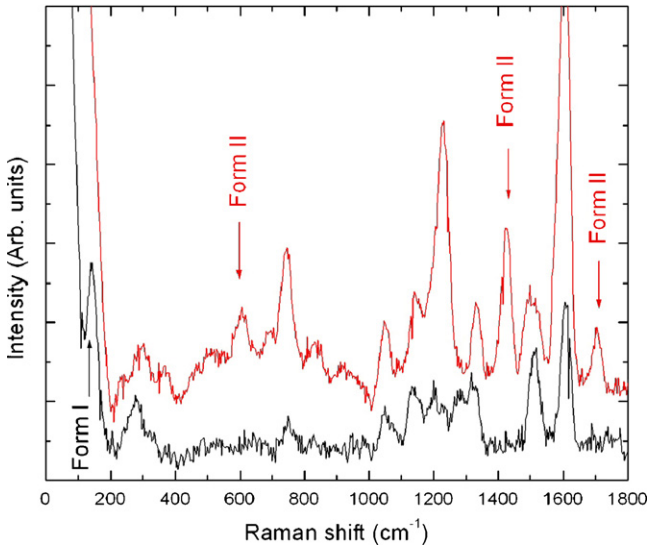

Fig. 7. Room temperature Raman spectra of forms I and II.

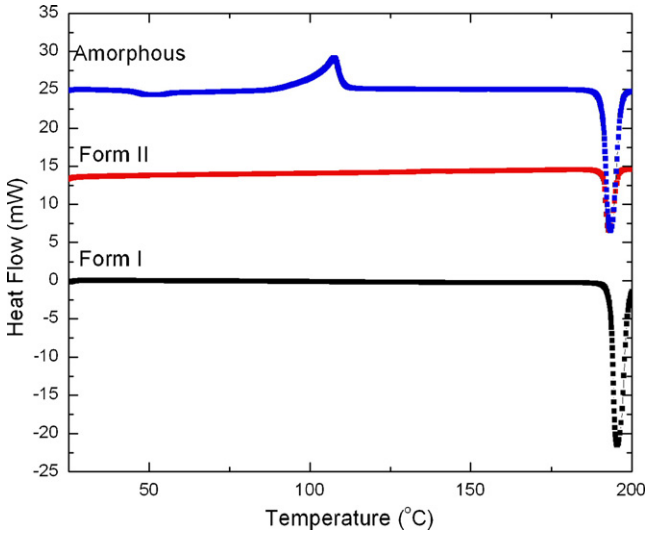

Fig. 8. Differential scanning calorimetry (DSC) of form I (bottom), form II (middle) and amorphous (top).

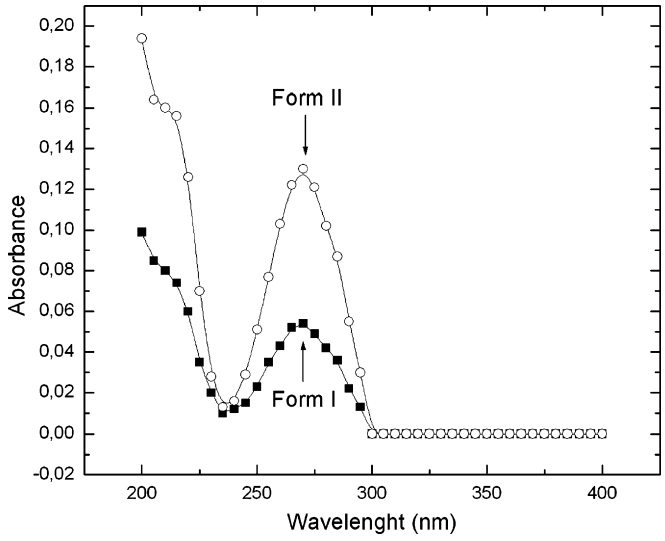

Fig. 9. UV–vis absorbance of water solution of form I (closed squares) and form II (open circles).

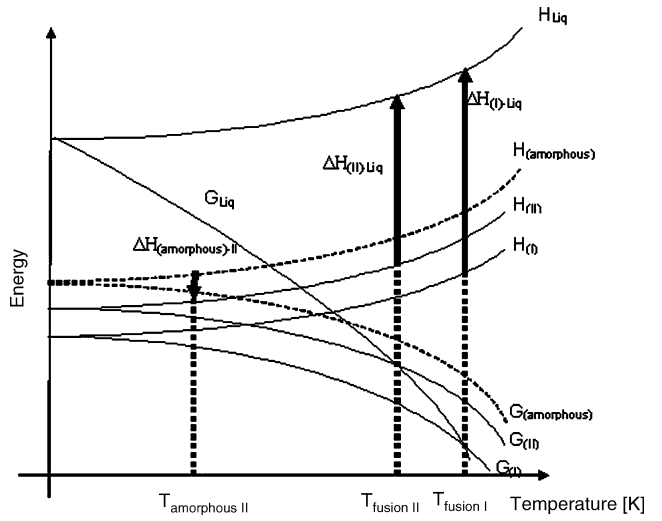

Fig. 10. Energy vs. temperature diagram. H and G for the amorphous phase are given as dashed lines because the behaviour of H and G was not studied above $T_{\text{amorphous II}}$.

Besides, the amorphous phase is very metastable and it converts to form II spontaneously at RT in around a week.

3.3. UV–vis absorbance

Fig. 9 presents the absorbance traces of saturated water solutions of forms I and II. A characteristic peak is observed around 270 nm, which is 2.4 times higher for form II than form I. These traces are a measurement of relative solubility of both polymorphs, so form II is more soluble than form I. The effect of polymorphism on solubility becomes especially critical because the rate of compound dissolution must also be dictated by the balance of attractive and disruptive forces existing at the crystal–solvent interface. A solid having a higher free energy (i.e., a less stable polymorph) will tend to dissolve faster, because the release of a higher amount of stored free energy will increase the solubility and hence the driven force for dissolution. In conclusion, form II is 2.4 times more soluble than form I, so form I is more stable and has less free energy. As can be expected, the solubility differences between both polymorphs enable a less stable form (form II in this case) to convert to the most stable one. However, no such conversion was observed in bicalutamide form II after 24 h in water suspension.

4. Discussion

A satisfactory explanation for these facts can be given considering forms I and II as a monotropic system (see Bernstein (2002) for details), where form I is considered the more stable one. Fig. 10 presents a schematic energy versus temperature diagram for such a case, where the four pairs of divergent curves represent the individual behaviours of the enthalpy (H) and the Gibbs free energy (G) for forms I, II, the amorphous phase and the liquid state.

In this diagram the $G_{(\text{II})}$ value for form II stays above the corresponding one for I all over the RT $-$ $T_{\text{fusion II}}$ (ca. 189 °C) range. The same behaviour has been observed for the amorphous phase respect to form II but not in an extended range of temperature. The amorphous samples suffer a glass transition around 50 °C (as expected according the rule of thumb where T_g is roughly (3/4)T_{fusion}, both temperatures are in K (Bernstein, 2002)), and after that an spontaneous transition to form II is observed. This transition is exothermic and $\Delta H_{\text{amorphous II}}$ is a measurement of the enthalpy difference between the amorphous phase and form II. It can be interpreted that the energy barrier between them is not high enough to avoid the spontaneous interconversion process in the solid state. In fact, the energy barrier is so low that spontaneous interconversion is observed at RT following a kinetic process quite slow (it lasted a week). The fact that amorphous phase converts to form II instead of form I can be explained thermodynamically by the Ostwald law, who formulated the law of successive reaction, that stated that "in all processes, it is not the most stable state with the lowest amount of free energy that is initially formed, but at least stable state lying nearest in free energy to the initial state" (Verna and Krishna, 1966).

Besides, taking into account that form I is the higher melting form, the proposed relative stability relation between forms I and II is also confirmed following the thermodynamics rules according to Buerger and Ramberger (1979a,b), because $\Delta H_{(\text{I})\,\text{Liq}}$ is greater than $\Delta H_{(\text{II})\,\text{Liq}}$, solubility of form I is lower than II and density of form I is greater than II.

5. Conclusions

The present results provide physical information to support an assignment of relative stability relationship between three structural modifications of Bicalutamide. In particular, the different thermal behaviours and the values of the measured magnitudes are shown in the energy versus temperature diagram.

As a final remark, it is perhaps worth emphasizing that the characterization presented above were the results of a combined analysis of complementary data obtained through a number of

multidisciplinary techniques (single crystal XRD, XRPD, DSC, Raman and UV–vis spectroscopy, etc.), none of which, on its own means, could have provide a definite answer to any of the question posed.

Acknowledgments

We acknowledge CONICET funding through project PIP 2367/00 and Universidad Nacional de General San Martín. DV thanks to Prof JAK Howard for the donation of the Rigaku AFC6S diffractometer.

References

Bernstein, J., 2002. Polymorphism in Molecular Crystals. Clarendon Press, Oxford.

Buerger, A., Ramberger, R., 1979a. On the polymorphism of pharmaceuticals and other molecular crystals. I. Theory of thermodynamic rules. Mikrochim. Acta (Wien) II, 259–271.

Buerger, A., Ramberger, R., 1979b. On the polymorphism of pharmaceuticals and other molecular crystals. II. Applicability of thermodynamic rules. Mikrochim. Acta (Wien) II, 273–316.

Caira, M.R., 1998. Crystalline polymorphism of organic compounds. Top. Curr. Chem. 198, 163–208.

Farrugia, L.J., 1999. WinGX. J. Appl. Cryst. 32, 837–838.

Haleblian, J., McCrone, W., 1969. Pharmaceutical applications of polymorphism. J. Pharm. Sci. 58 (8), 911–929.

MSC/AFC, 1993. Diffractometer Control Software, Version 4.3.0. Molecular Structure Corporation, The Woodlands, TX, USA.

Sheldrick, G.M., 1994. SHELXTL-PC, Version 5.0. Siemens Analytical X-ray Instruments Inc., Madison, WI, USA.

Sheldrick, G.M., 1997. SHELXS97 and SHELXL97. University of Göttingen, Germany.

US Patent 6,740,770 B2 (May 25, 2004).

Verna, A.R., Krishna, P., 1966. Polymorphism and Polytypism in Crystals. John Wiley, New York, pp. 15–30.

WO A1 Patent 2004/029201 A1 (April 8, 2004).

WO A2 Patent 2004/074350 A2 (September 2, 2004).

Yu, L., Reutzel-Edens, S.M., Mitchel, C.A., 2000. Crystallization and polymorphism of conformationally flexible molecules: problems, patterns, and strategies. Org. Proc. Research and Dev. 4 (5), 396–402.